

# Energy determination in the Akeno Giant Air Shower Array experiment

M. Takeda<sup>a</sup>, N. Sakaki<sup>a</sup>, K. Honda<sup>b</sup>, M. Chikawa<sup>c</sup>,  
 M. Fukushima<sup>d</sup>, N. Hayashida<sup>d</sup>, N. Inoue<sup>e</sup>, K. Kadota<sup>f</sup>,  
 F. Kakimoto<sup>g</sup>, K. Kamata<sup>h</sup>, S. Kawaguchi<sup>i</sup>, S. Kawakami<sup>j</sup>,  
 Y. Kawasaki<sup>a</sup>, N. Kawasumi<sup>k</sup>, A. M. Mahrous<sup>e</sup>, K. Mase<sup>d</sup>,  
 S. Mizobuchi<sup>l</sup>, Y. Morizane<sup>d</sup>, M. Nagano<sup>m</sup>, H. Ohoka<sup>d</sup>,  
 S. Osone<sup>d</sup>, M. Sasaki<sup>d</sup>, M. Sasano<sup>n</sup>, H. M. Shimizu<sup>a</sup>,  
 K. Shinozaki<sup>d</sup>, M. Teshima<sup>d</sup>, R. Torii<sup>d</sup>, I. Tsushima<sup>k</sup>,  
 Y. Uchihori<sup>o</sup>, T. Yamamoto<sup>d</sup>, S. Yoshida<sup>p</sup>, and H. Yoshii<sup>l</sup>

<sup>a</sup> *RIKEN (The Institute of Physical and Chemical Research), Saitama 351-0198, Japan*

<sup>b</sup> *Faculty of Engineering, Yamanashi University, Kofu 400-8511, Japan*

<sup>c</sup> *Department of Physics, Kinki University, Osaka 577-8502, Japan*

<sup>d</sup> *Institute for Cosmic Ray Research, University of Tokyo, Chiba 277-8582, Japan*

<sup>e</sup> *Department of Physics, Saitama University, Urawa 338-8570, Japan*

<sup>f</sup> *Faculty of Engineering, Musashi Institute of Technology, Tokyo 158-8557, Japan*

<sup>g</sup> *Department of Physics, Tokyo Institute of Technology, Tokyo 152-8551, Japan*

<sup>h</sup> *Nishina Memorial Foundation, Komagome, Tokyo 113-0021, Japan*

<sup>i</sup> *Faculty of Science and Technology, Hirosaki University, Hirosaki 036-8561, Japan*

<sup>j</sup> *Department of Physics, Osaka City University, Osaka 558-8585, Japan*

<sup>k</sup> *Faculty of Education, Yamanashi University, Kofu 400-8510, Japan*

<sup>l</sup> *Department of Physics, Ehime University, Matsuyama 790-8577, Japan*

<sup>m</sup> *Department of Space Communication Engineering, Fukui University of Technology, Fukui 910-8505, Japan*

<sup>n</sup> *Communications Research Laboratory, Ministry of Posts and Telecommunications, Tokyo 184-8795, Japan*

<sup>o</sup> *National Institute of Radiological Sciences, Chiba 263-8555, Japan*

<sup>p</sup> *Department of Physics, Chiba University, Chiba 263-8522, Japan*

---

**Abstract**

Using data from more than ten-years of observations with the Akeno Giant Air Shower Array (AGASA), we published a result that the energy spectrum of ultra-high energy cosmic rays extends beyond the cutoff energy predicted by Greisen [1], and Zatsepin and Kuzmin [2]. In this paper, we reevaluate the energy determination method used for AGASA events with respect to the lateral distribution of shower particles, their attenuation with zenith angle, shower front structure, delayed particles observed far from the core and other factors. The currently assigned energies of AGASA events have an accuracy of  $\pm 25\%$  in event-reconstruction resolution and  $\pm 18\%$  in systematic errors around  $10^{20}$  eV. This systematic uncertainty is independent of primary energy above  $10^{19}$  eV. Based on the energy spectrum from  $10^{14.5}$  eV to a few times  $10^{20}$  eV determined at Akeno, there are surely events above  $10^{20}$  eV and the energy spectrum extends up to a few times  $10^{20}$  eV without a GZK-cutoff.

*Key words:* Extensive air showers, ultra high energy cosmic rays, energy determination

*PACS:* 96.40.Pq, 95.55.Vj, 96.40.De, 95.85.Ry

---

## 1 Introduction

From ten-years of data collected by the Akeno Giant Air Shower Array (AGASA), we have shown that the energy spectrum of primary cosmic rays extends up to a few times  $10^{20}$  eV without the expected GZK cutoff [3]. On the other hand, the HiRes collaboration has recently claimed that the GZK cutoff may be present with their exposure being similar to AGASA [4]. Ave et al. [5] have re-analyzed the Haverah Park events and their energies are reduced by about 30% using a new energy conversion formula. Although we have already published our statistical and systematic errors in the energy determination in related papers [3,6,7,8], it is now quite important to reevaluate uncertainties in the energy determination of AGASA events with the accumulated data of ten years. The uncertainties due to shower front structure and delayed particles far from a shower core are also evaluated and described in some detail.

The AGASA array is the largest operating surface array, covering an area of about  $100\text{km}^2$  and consisting of 111 surface detectors of  $2.2\text{m}^2$  area [9,10]. Each surface detector is situated with a nearest-neighbor separation of about 1km and the detectors are sequentially connected with pairs of optical fibers. All detectors are controlled at detector sites with their own CPU and through rapid communication with a central computer. In the early stage of our experiment AGASA was divided into four sub-arrays called “branches” for topographical reasons, and air showers were observed independently in each branch. The

data acquisition system of AGASA was improved and the four branches were unified into a single detection system in December 1995 [11]. After this improvement the array has operated in a quite stable manner with a duty cycle of about 95%, while the duty cycle before unification was 89%.

In a widely spread surface array like AGASA, the local density of charged particles at a specific distance from the shower axis is well established as an energy estimator [12] since the local density of the electromagnetic component depends weakly on variations in interaction models, fluctuations in shower development and primary mass. In the AGASA experiment, we adopt the local density at 600m,  $S(600)$ , which is determined by fitting a lateral distribution function (LDF) of observed particle densities to an empirical formula [7]. This empirical formula is found to be valid for EAS with energies up to  $10^{20}$ eV and for zenith angles smaller than  $45^\circ$  [13,14]. The relation for converting  $S(600)$  to primary energy is evaluated by Monte Carlo simulations [15] up to  $10^{19}$ eV and is

$$E = 2.03 \times 10^{17} \cdot S_0(600) \quad \text{eV} \quad , \quad (1)$$

where  $S_0(600)$  is the  $S(600)$  value per  $\text{m}^2$  for a vertically incident shower. This conversion relation is derived from electron components for air showers observed 900m above sea level. In §3.3, a new conversion relation is presented and we take into account the average altitude of the array (667m).

In the southeast corner of AGASA there is the Akeno  $1\text{km}^2$  array [16]. This is a densely packed array of detectors covering an area of  $1\text{km}^2$  operated since 1979. This array was used to determine the energy spectrum between  $10^{14.5}$ eV and  $10^{18.5}$ eV. In this experiment, the total number of electrons, known as the shower size  $N_e$ , was used as an energy estimator. The relation between this energy spectrum and the AGASA energy spectrum is discussed in §4.

## 2 Densities measured by scintillation detectors

The AGASA array consists of plastic scintillators of  $2.2\text{m}^2$  area, and the light from these scintillators is viewed by a 125mm diameter Hamamatsu R1512 photomultiplier tube (PMT) at the bottom of each enclosure box. The scintillators are 5cm thick (0.14 radiation lengths). The enclosure box and a detector hut are made of steel with 2mm and 0.4mm thickness, respectively. There is another type of enclosure box used for 17 detectors in the Akeno branch, in which PMT is mounted at the top of each enclosure box.

In order to cover a dynamic range from 0.3 to a few times  $10^4$  particles per detector, a logarithmic amplifier is used [9]. The number of incident particles

is determined from the pulse width, which is obtained by presenting such a signal that decays exponentially with a time constant of  $\tau \simeq 10\mu s$  to a discriminator with a constant threshold level  $V_d$ . The relation between the number of incident particles  $N$  and the pulse width  $t_d$  is given by

$$V_d = V e^{-t_d/\tau} = kN e^{-t_d/\tau} \quad , \quad (2)$$

where  $V$  is the pulse height ( $V = kN$ ,  $k$  is a constant depending on the gain of the amplifier). By defining the pulse width for  $N = 1$  as  $t_1$ , one obtains

$$\ln N = \frac{t_d - t_1}{\tau} \quad . \quad (3)$$

Figure 1 shows a typical pulse width distribution (PWD) for omni-directional muons, and its peak value  $PW_{peak}^\theta$  is used as  $t_1$ .

In the Akeno experiment, the original definition of a ‘‘single particle’’ was based on the average value ( $PH_{ave}^0$ ) of a pulse height distribution (PHD) from muons traversing a scintillator vertically [17]. This  $PH_{ave}^0$  is accidentally coincident with the peak value  $PH_{peak}^\theta$  of the PHD of omni-directional muons, since the PHD is not a Gaussian distribution but is subject to Landau fluctuations. The parameter  $PH_{peak}^\theta$  is related to  $PW_{peak}^\theta$  by

$$PW_{peak}^\theta = \frac{1}{2} \left( PH_{peak}^\theta + \sqrt{PH_{peak}^{\theta 2} + \sigma^2} \right) \quad , \quad (4)$$

where  $\sigma$  is the full width at half maximum of the PHD [18]. With  $PH_{peak}^\theta = 1.0$  and  $\sigma = 0.7$ ,  $PW_{peak}^\theta = 1.1$ . The density measured in units of  $PW_{peak}^\theta$ , therefore, is 1.1 times smaller than that measured in units of  $PH_{peak}^\theta (= PH_{ave}^0)$ . On the other hand, the density measured with a scintillator in units of  $PH_{ave}^0$  is 1.1 times larger than the electron density measured with spark chambers between 10m and 100m from shower cores [19]. This means that the density in units of  $PW_{peak}^\theta$  corresponds to an electron density measured by a spark chamber, given that the ratio of densities measured with scintillators and spark chambers is 1.1. The number of particles in units of  $PW_{peak}^\theta$ , therefore, coincides with the true electron density and has been applied to estimate primary energy using Equation (1).

### 3 Evaluation of uncertainties on energy estimation in AGASA

#### 3.1 Detector

The detector positions were measured using a stereo camera from an air-plane with accuracies of  $\Delta X, \Delta Y = 0.1\text{m}$  and  $\Delta Z = 0.3\text{m}$ . The cable lengths (the propagation delay times of signals) from the Akeno Observatory to each detector is regularly measured with accuracy of 0.1ns in each RUN (about twice a day). Figure 2 shows the variation in cable length for a typical detector as a function of day. A discontinuity around 50,000 MJD is due to the movement of the detector position and another one is due to the system upgrade in 1995.

In Equation (3), there are two parameters which should be determined. The first one is the ‘‘single particle’’  $t_1$  ( $= PW_{peak}^\theta$ ). In the AGASA experiment, pulse widths of all incident particles are recorded and their PWD is stored in the memory as shown in Figure 1, and then  $t_1$  is determined in every RUN. Figure 3(a) shows the time variation of  $t_1$  for a typical detector over 11-years of operation. There is a clear seasonal variation with a  $\pm 3\%$  fluctuation, but this variation has been calibrated in the air shower analysis using monthly data. The variance  $\sigma^2(t_1)$  within each month of data is determined and  $\sigma(t_1)$  is shown for all detectors in Figure 3(b), with  $\sigma(t_1)/\langle t_1 \rangle \leq 0.7\%$  for a 68% C.L.

The second important parameter is the decay constant  $\tau$ . Although we have directly measured the  $\tau$  values with a LED several times during AGASA’s operation, they are not enough to estimate the time variation of  $\Delta\tau/\tau$ . We estimate this variation using the observed PWDs. Assuming the density (particle number) spectrum of incident particles in a detector is  $I \propto N^{-\gamma}$ , one obtains

$$\Delta \ln I = -\gamma \frac{\Delta N}{N} = -\gamma \frac{\kappa \Delta x}{\tau} \quad (t_d = \kappa x) \quad . \quad (5)$$

The ratio  $a \equiv \Delta \ln I / \Delta x$  is the slope of the PWD, so that the ratio  $\Delta\tau/\tau$  is expressed by

$$\frac{\Delta\tau}{\tau} = -\frac{\Delta a}{a} \quad . \quad (6)$$

Figure 4(a) shows the time variation in  $\Delta a/a$  for a typical detector. The variance  $\sigma^2(\frac{\Delta a}{a})$  is determined throughout the observation time (11 years) for each detector. For all 111 detectors,  $\sigma(\frac{\Delta a}{a})$  is plotted in Figure 4(b), and  $\sigma(\frac{\Delta a}{a})/\langle \frac{\Delta a}{a} \rangle \leq 1.6\%$  at a 68% C.L. This fluctuation causes an uncertainty in

density estimation of 4% for 10 particles and 7% for 100 particles per detector. It should be noted that  $\sigma(\frac{\Delta a}{a})$  includes not only the change of  $\tau$  but also that of  $\gamma$  caused by varying atmospheric conditions (temperature and pressure). The real variation in  $\Delta\tau/\tau$  is, therefore, smaller than that for  $\Delta a/a$  discussed above.

To confirm whether a “single particle” is appropriate, the CORSIKA program has been used to simulate densities measured by a scintillator of a 5cm thickness [20]. In this simulation, a “single particle” corresponds to  $PH_{ave}^0$ . Figure 5 plots the lateral distribution of energy deposit in the scintillator in units of  $PH_{ave}^0$  (closed circles), and it is compared with the experimental LDF (dashed curve). The simulated LDF is flatter than the experimental one. The simulated density reflects the number of electrons near the core (up to about 200m from the core), but becomes larger than the electron density with increasing core distance. Recently we have also studied the detector response with the GEANT simulation [21,22]. In this simulation, a “single particle” is defined as the peak value of  $\log_{10}(\text{energy deposit in scintillator})$  for omnidirectional muons with their energy spectrum to represent the experimental  $PW_{peak}^\theta$ . Here we take account of the real configuration of a detector, conversion of photons in the wall of the enclosure box and the detector hut, scattering of particles, decay of unstable particles (pions, kaons and etc), and the 4-momentum of shower particles. The shape of the lateral distribution is nearly consistent with the experimental LDF, though it is also a little flatter than the experimental one. With these simulation studies, we have also studied  $S(600)$  for another type of enclosure box used for 17 detectors in the Akeno branch. The difference is within 5% in density measurement for various energy and zenith angle ranges.

### 3.2 Air Shower Phenomenology

#### (a) Lateral Distribution Function:

The empirical formula of the LDF [7] is expressed by

$$\rho(r) \propto \left(\frac{r}{R_M}\right)^{-1.2} \left(1 + \frac{r}{R_M}\right)^{-(\eta-1.2)} \left\{1 + \left(\frac{r}{1000}\right)^2\right\}^{-0.6}, \quad (7)$$

where  $r$  is the distance from the shower axis in meters. The Moliere unit  $R_M$  is 91.6m at the Akeno level. The parameter  $\eta$  indicates the slope index of the LDF at  $r > R_M$  and is a function of zenith angle  $\theta$  expressed by

$$\eta = (3.97 \pm 0.13) - (1.79 \pm 0.62) (\sec \theta - 1) \quad . \quad (8)$$

The uncertainty in the energy determination of showers due to the limited accuracy in determination of  $\eta$  was discussed and estimated to be  $\pm 10\%$

by Yoshida et al. [7].

With observed showers, we have confirmed that the empirical formula of Equations (7) and (8) can be applied to showers with energies up to  $10^{19.8}\text{eV}$  and with core distances up to 3km [22]. In the same manner as Yoshida et al. [7], the systematic effect on  $S(600)$  estimation due to uncertainties in Equation (8) is evaluated to be  $\pm 7\%$  for air showers with zenith angles smaller than  $45^\circ$ .

(b) Atmospheric Attenuation:

Since an inclined air shower traverses the atmosphere deeper than a vertical shower, a shower density  $S_\theta(600)$  observed at zenith angle  $\theta$  must be transformed into  $S_0(600)$  corresponding to a vertical shower. The attenuation of  $S_\theta(600)$  is formulated as follows:

$$S_\theta(600) = S_0(600) \exp \left[ -\frac{X_0}{\Lambda_1}(\sec \theta - 1) - \frac{X_0}{\Lambda_2}(\sec \theta - 1)^2 \right] \quad , \quad (9)$$

where  $X_0 = 920\text{g/cm}^2$ ,  $\Lambda_1 = 500\text{g/cm}^2$  and  $\Lambda_2 = 594_{-120}^{+268}\text{g/cm}^2$  for  $\theta \leq 45^\circ$  [7]. The uncertainty in  $S(600)$  determination due to the uncertainty in the attenuation curve of  $S(600)$  was also discussed there.

The attenuation curve of  $S(600)$  is now under reevaluation with the accumulated data up to zenith angles  $\theta \leq 60^\circ$ . For events with  $\theta \leq 45^\circ$ , Equation (9) can be used and the uncertainty in  $S_0(600)$  due to this transformation is estimated to be  $\pm 5\%$ ; this value is also reduced from Yoshida et al. [7] because of the increased amount of observed showers.

(c) Accidental Coincidence:

Because we use the log-amplifier described above, the density could be overestimated if an accidental signal hits on the tail of the exponential pulse above the threshold level of the discriminator. The counting rate of the scintillation detector (area  $2.2\text{m}^2$ ) is about 500Hz for signals exceeding the threshold of 0.3 particles per detector. The accidental coincidence of a background particle hitting a detector within the pulse of a single particle ( $10\mu\text{s}$  width) occurs with a chance probability of  $10 \times 10^{-6} \times 500 = 5 \times 10^{-3}$ . In the same way, one obtains  $1.65 \times 10^{-2}$  for the probability during a 10 particle pulse ( $33\mu\text{s}$  width) and  $5.6 \times 10^{-2}$  for a 100 particle pulse ( $56\mu\text{s}$  width). This means that one of 200, 61, or 18 detectors in each case may record larger values than the real density. With the present analysis method described in §3.4, a detector which deviates more than  $3\sigma$  from the average LDF is excluded and hence this effect is negligible.

(d) Shower Front Structure:

Given our use of the log-amplifier, the density is properly estimated so long as the thickness of a shower front is less than a few 100ns. However, if the thickness is larger than this time width, we should take this effect into account to estimate the incident particle density appropriately. Figure 6 is an example of the arrival time distribution observed with a  $30\text{m}^2$  scintillator [6], operated by the Yamanashi university group and triggered

by AGASA. The core distance is 1,920m and the primary energy is  $2 \times 10^{20}$ eV. Not only is the particle arrival time distribution broad, but 5 particles are delayed more than  $3\mu\text{s}$  in this  $30\text{m}^2$  detector.

The arrival time distribution of shower particles has been measured with a scintillation detector of  $12\text{m}^2$  area together with the  $30\text{m}^2$  detector. Signal sequences of arriving particles are recorded in time bins of 50ns for the  $30\text{m}^2$  detector and 20ns for the  $12\text{m}^2$  detector in coincidence with the AGASA trigger. The details of these experiments are described in Honda et al. [23,24]. From these experiments, the average shape of the arrival time distribution is expressed by

$$f(t, r) = \frac{t}{t_0(r)} \exp\left(\frac{-t}{t_0(r)}\right) \quad , \quad (10)$$

where the scaling parameter  $t_0$  is 168ns, 212ns, and 311ns at  $r = 534\text{m}$ ,  $750\text{m}$ , and  $1,050\text{m}$ , respectively. These are shown by solid lines in Figure 7. Beyond  $1,050\text{m}$  the events are too few to determine the average  $t_0$ . However, if we extrapolate the relation assuming  $\log t_0 \propto r$ , we find  $t_0 = 490\text{ns}$  at  $r = 1,500\text{m}$  and  $850\text{ns}$  at  $2,000\text{m}$ . The arrival time distribution of events in these distant ranges seems to be rather shorter than these values (K.Honda, private communication) and the above  $t_0$  values may be upper bounds up to  $2,000\text{m}$  and for events with energies up to  $10^{20}\text{eV}$ . These distributions are also drawn with dotted lines in Figure 7. The solid curves in Figure 6 correspond to the time distribution with  $t_0 = 800\text{ns}$ , which support the extrapolation with  $\log t_0 \propto r$ .

Using  $t_0$  and the number of incident particles as parameters, we have derived the ratio (the overestimation factor) of the estimated density due to the broadening of the shower front structure to the density with  $t_0 = 0$  as a function of core distance and primary energy. The results are drawn in Figure 8. The factor is nearly independent of primary energy up to a few  $1,000\text{m}$ . The factor increases rapidly with core distance above  $1,500\text{m}$ , but it decreases suddenly again at those core distances where the observed number of shower particles is near unity. From this figure, the overestimation factor for the density at  $600\text{m}$  is  $+3.5\%$  and that around  $1\text{km}$  is  $+6\%$  for  $10^{20}\text{eV}$  showers. With our analysis method described in §3.4, the present  $S(600)$  may be overestimated by about  $5\%$  due to the broadening of the shower front structure with its fluctuation about  $\pm 5\%$ .

(e) Delayed Particles:

As shown in Figure 6, there are particles at large core distances which are delayed by more than a few micro seconds with respect to normal shower particles. It was shown in the prototype AGASA experiment that pulses delayed by more than  $4\mu\text{s}$  are most likely to be low energy neutrons with energy  $30\text{--}40\text{MeV}$  and the fraction of these pulses to the total shower particles is a few % between  $1\text{km}$  and  $3\text{km}$  [25]. Based on this result, we have so far assumed that the effect of delayed particles on the  $S(600)$



determination is within the errors due to other effects.

In the following, we evaluate the effect of delayed particles on the  $S(600)$  determination with accumulated data from ten years of operation. If a delayed particle, whose energy loss in a scintillator corresponds to  $N_D$  particles, hits a detector with time delay  $t_D$  with respect to  $N_i$  incident particles at  $t = 0$ , the pulse height  $V(t)$  is expressed by

$$V(t) = N_i \exp\left(-\frac{t}{\tau}\right) + N_D \exp\left(-\frac{t-t_D}{\tau}\right) = OF \cdot N_i \exp\left(-\frac{t}{\tau}\right) \quad (11)$$

$$OF = 1 + \frac{N_D}{N_i} \exp\left(\frac{t_D}{\tau}\right) \quad ,$$

where  $N_i$  and  $N_D$  are in units of a “single particle”, and  $OF$  is the over-estimation factor due to delayed particles. The  $OF$  value depends on  $N_D/N_i$  and  $t_D$ . It is, therefore, quite important to evaluate the density of delayed particles and their energy loss in a 5cm scintillator experimentally. These values have been measured with the scintillation detectors of 30m<sup>2</sup> and 12m<sup>2</sup> area described in the previous section.

Figure 9 shows the ratio of delayed particles (delay time  $t_D \geq 3\mu\text{s}$  and pulse height  $N_D \geq 1.0$  particles) to all shower particles measured as a function of core distance for three energy ranges:  $\log(\text{Energy [eV]}) = 18.5\text{--}19.0$  (open circles),  $19.0\text{--}19.4$  (open squares) and above 19.4 (closed squares). In the same figure, the previous Akeno result by Teshima et al. [25] and the result by Linsley [26] are also plotted by small open and closed circles, respectively. In these measurements, ratios of delayed particles with delay time  $t_D \geq 4\mu\text{s}$  and pulse height  $N_D \geq 3.0$  particles to all particles are plotted for showers of energies around  $10^{18}\text{eV}$ . When we take account of the different selection conditions it may be concluded that the ratio of the number of delayed particles to all shower particles depends on core distance, and is almost independent of primary energy from  $10^{18}\text{eV}$  to  $10^{20}\text{eV}$ .

Figure 10 shows the ratio  $N_D/N_i$  as a function of core distance observed by the 30m<sup>2</sup> or 12m<sup>2</sup> detectors. Here,  $N_D$  represents the energy loss in scintillators of the delayed particles (delay time  $t_D \geq 3\mu\text{s}$  and pulse height  $N_D \geq 1.0$  particles) measured in units of  $PH_{ave}^0$ , and  $N_i$  is sum of all shower particles also in units of  $PH_{ave}^0$  for showers in the same distance and energy bin. Open circles represent the ratio for showers of energies between  $10^{18.5}\text{eV}$  and  $10^{19.0}\text{eV}$ , and closed squares for energies above  $10^{19.0}\text{eV}$ .

In Figure 11, the delay time and  $N_D$  of a delayed particle (units of  $PH_{ave}^0$ ) are plotted as a function of core distance. Since there is no appreciable difference for different primary energies, delayed particles for all energy ranges are put together in this analysis. Details of the shower front structure and delayed particles will be described elsewhere [27].

Using the  $N_D/N_i$  values in Figure 10 and the delay times in Figure 11,

the  $OF$  values are estimated from Equation (11) and plotted in Figure 12 as a function of core distance. These  $OF$  values are independent of primary energy. This is understood as follows. For  $10^{19}$ eV showers, the density at a core distance of 1km is  $6/\text{m}^2$  (for AGASA detector  $N_i = 13.2/2.2\text{m}^2$ ), so that the density overestimation  $OF$  due to delayed particles with  $N_D = 3$  is expected to be 1.31 for  $t_D = 3\mu\text{s}$  and 1.37 for  $t_D = 5\mu\text{s}$ . However, the density of the delayed particles is so small that only one in 10 detectors around 1km will be hit by delayed particles. Since the average density is determined by several detectors, the  $S(600)$  overestimation is limited to 4%. On the other hand, for  $10^{20}$ eV showers all detectors around 1km from the air shower core are likely to be hit by delayed particles. However, the density overestimation ( $OF$ ) of each detector is 1.04 because the density of shower particles around 1km is large ( $N_i = 132$ ) at  $10^{20}$ eV.

From our analysis procedure described in §3.4,  $S(600)$  may be overestimated due to delayed particles by about  $+5\% \pm 5\%$ , independent of primary energy. It should be noted that the AGASA LDF is consistent with that from electromagnetic components and muons simulated as described in §3.1. If we include the simulated results on low energy neutrons (delayed particles) using AIRES code, the LDF becomes much flatter than the observed LDF beyond 1km from the core. A possible flattening of LDF due to delayed particles is not observed experimentally up to 3km from the core and up to  $10^{20}$ eV.

### 3.3 Energy Estimator

The particle density  $S_0(600)$  in Equation (1) is evaluated as the electron density and the AGASA density in units of  $PW_{peak}^\theta$  corresponds to the electron density since the ratio of densities measured with scintillators and a spark chamber is 1.1 as described in §2. Since this ratio is not measured beyond 100m, it is necessary to evaluate the conversion factor from  $S(600)$  measured in units of the AGASA “single particle” to primary energy.

The new conversion formula obtained is described in Sakaki et al.[22] and listed in Table 1. In this simulation a “single particle” is defined as  $PW_{peak}^\theta$  in accordance with the experiment. The energy conversion formula of Equation (1) was estimated for the 900m altitude of the Akeno Observatory. Since the Akeno Observatory is located on a mountain side, core positions of most events are lower than this altitude. At the average 667m height of the AGASA detectors, the atmospheric depth is  $27\text{g}/\text{cm}^2$  larger than that at the Akeno Observatory. In the new simulation, this altitude is applied.

If we evaluate the difference in a factor  $a$  in Table 1 due to the difference

of average altitudes 900m and 667m, it leads to a 7% increase at  $S(600) = 1$ . That is, Equation (1) evaluated at 900m is revised to

$$E = 2.17 \times 10^{17} \cdot S_0(600)^{1.0} \quad \text{eV} \quad , \quad (12)$$

at 667m and the result agrees with the factor  $a$  calculated using the QGSJET interaction model and a proton primary by Sakaki et al. [21] in Table 1.

In order to see the differences due to simulation codes and hadronic interaction models, the simulation by Nagano et al. [20] using CORSIKA is also listed. In this simulation, the density in units of  $PH_{peak}^0$  is used and the average altitude is 900m. Taking account of 10% overestimation of a “single particle” ( $PH_{peak}^0$ ) and the 7% underestimation due to differences in altitude, we may directly compare these results with Sakaki et al. [21]. In each simulation, the differences are within 10% between QGSJET and SIBYLL hadronic interaction models and are within 10% between proton and iron primaries. The difference due to the simulation code itself is within 5%.

It is, therefore, reasonable to use a revised energy conversion formula by taking the average of these simulation results at 667m for proton and iron primaries with AIRES (QGSJET, SIBYLL), CORSIKA (QGSJET, SIBYLL) and COSMOS (QCDJET) yielding

$$E = 2.21 \times 10^{17} \cdot S_0(600)^{1.03} \quad \text{eV} \quad . \quad (13)$$

That is, the AGASA energies so far published must be shifted by +8.9% at  $2 \times 10^{17}$ eV, +12.2% at  $10^{19}$ eV and +13.1% at  $10^{20}$ eV. The systematics due to the simulation codes, interaction models, and mass composition may be within 10%. The intrinsic  $S(600)$  fluctuation in shower development is less than 6% under each combination of primary mass and interaction model with the AIRES simulation [22]. This small difference among interaction models and compositions is an advantage of measuring  $S(600)$  using scintillators, in which observed particles are dominated by electromagnetic components with a small contribution of muons.

From the above discussion, Equation (1) used so far by the AGASA group gives the lowest limit in the conversion from  $S(600)$  to primary energy. It may be more reasonable to increase the energies +10%  $\pm$ 12%. A detailed study of this topic will be found in [22].

### 3.4 Analysis

Our analysis procedure for an air shower event is based on an iterative process to find the arrival direction of a primary cosmic ray and to search for the core location and the local density  $S(600)$ . To start, we assume an initial core location at the center of gravity of the density distribution of an observed event. Next, the arrival direction is determined by minimizing the  $\chi^2$  function:

$$\chi^2 = \frac{1}{n-3} \sum_{i=1}^n \left[ \{T_i - T_f - T_d - T_0\}^2 / T_s^2 \right] \quad . \quad (14)$$

Here,  $T_i$  is the observed time of the first particle incident on  $i$ -th detector,  $T_f$  is the propagation time of the tangential plane of the shower front,  $T_d$  is the average time delay of the shower particles from the tangential plane,  $T_s$  is the average deviation of shower particles, and  $T_0$  denotes the time when the core hits the ground. The parameters ( $T_d$  and  $T_s$ ) of shower front structure are obtained experimentally [28]. At this step, those detectors that make  $\chi^2$  large are excluded in the calculation as signals with accidental muons. This exclusion is continued until  $\chi^2 \leq 5.0$ . Usually, the number of excluded detectors is one or a few. In the next step, we search for the core location and the shower size, which corresponds to the normalization factor in Equation (7), to maximize the likelihood function:

$$\mathbb{L} = \prod_{i=1}^n \left( \frac{1}{\sigma_i \sqrt{2\pi}} \right) \cdot \exp \left[ -\frac{1}{2} \sum_{i=1}^n \left( \frac{\rho_i - \rho(R_i)}{\sigma_i} \right)^2 \right] \quad , \quad (15)$$

where  $\rho_i$  is the electron density observed by  $i$ -th detector and  $\rho(R_i)$  is the particle density estimated from the LDF. The fluctuation of electron density  $\sigma_i$  takes account of fluctuations in the longitudinal development and the detector response. This fluctuation was experimentally expressed by Teshima et al. [25]. At this step, we again exclude a detector if its observed density deviates by more than  $3\sigma$ , and we assume these signals are possibly overestimated by an accidental coincidence or delayed particles. Finally, we estimate the local density  $S_\theta(600)$  and convert it to the primary energy.

Figure 13 shows the distributions of energies evaluated using the above analysis method for a large number of artificial proton air shower events simulated with energies of  $3 \times 10^{19}$  eV and  $10^{20}$  eV at zenith angles less than  $45^\circ$ . For artificial events above  $10^{19}$  eV and  $4 \times 10^{19}$  eV, 68% have accuracy in arrival direction determination better than  $2.8^\circ$  and  $1.8^\circ$ , respectively. These artificial events were simulated over a larger area than the AGASA area with directions sampled from an isotropic distribution. In this air shower simulation, the fluctuation on the longitudinal development of air showers, the resolution of the

scintillation detectors, and the statistical fluctuation of observed shower particles at each surface detector were taken into account. The primary energy is determined with an accuracy of about  $\pm 30\%$  at  $3 \times 10^{19}\text{eV}$  and  $\pm 25\%$  at  $10^{20}\text{eV}$ , and the fraction of events with 50%-or-more overestimation in energy is only 2.4%.

Although only events whose cores are located within the array area are used in our papers, some events with real cores located near but outside the array boundary are reconstructed as “inside” events. The assigned energies of such events are smaller than their real values since the core distance of detectors become nearer than the true distances. On the other hand, such events that are assigned “outside” the array boundary in the analysis procedure against their input core locations inside the array are excluded in our selection. The effects from these mislocation of cores are taken into account in the distributions in Figure 13 and the exposure in Figure 14.

#### 4 AGASA energy spectrum and the relation to that in lower energy determined at Akeno

In order to derive the energy spectrum of primary cosmic rays, the observation time and the aperture for the selected events must be evaluated as a function of the primary energy. The observation time is  $2 \times 10^5$  hours up to July 2001. The aperture is determined by analyzing the artificial showers simulated over an area larger than the AGASA area described above.

Figure 14 shows the energy spectrum observed with AGASA with zenith angles smaller than  $45^\circ$  up until July 2001. The exposure (the aperture  $\times$  the observation time) is also drawn in Figure 14 and is almost constant at  $4.6 \times 10^{16}\text{m}^2 \text{ s sr}$  above  $10^{19}\text{eV}$  for the events inside the array boundary. Closed circles indicate these “inside” events, and open circles are “well contained” events whose cores are located at least 1km inside the array boundary. The energy spectra for inside and well contained events agree well with each other and hence our criterion of selecting all events inside the boundary can be justified.

Though we have examined the systematic errors in energy determination carefully, it is not easy to calibrate the absolute energy experimentally to decide whether  $10^{20}\text{eV}$  candidate events really exceed the GZK cutoff energy. One method is to compare the spectrum with the extension of Akeno energy spectrum measured at lower energies. At Akeno there are arrays of various detector-spacing depending on the primary energy of interest, and energy spectra have been determined systematically over five decades in energy under the similar experimental procedures [29].

In the  $10^{18}$ eV energy region, a comparison of energy determination using  $S(600)$  and  $N_e$  for each event can be made with the  $1\text{km}^2$  array, where 156 detectors of  $1\text{m}^2$  area each are arranged with 120m separation. One of the largest events hitting the  $1\text{km}^2$  array is shown in Figure 15, with energies estimated from the shower size  $N_e$  and  $S(600)$ . The relation converting  $N_e$  to energy at Akeno is determined experimentally via the longitudinal development curve measured at Chacaltaya and Akeno [29]. Though the number of events above  $10^{18}$ eV is small, the difference in energy determined using both methods is within 10%. In other words, the energy conversion factor from  $S(600)$  by simulation is in good agreement with that from  $N_e$  by experiment.

The energy determined by the  $1\text{ km}^2$  array ( $E_1$ ) and that by the  $20\text{km}^2$  array ( $E_{20}$ ), whose detectors are deployed with about 1km separation and is the prototype array of AGASA, have also been compared in the  $10^{18}$ eV energy region [30]. The ratio  $E_{20}/E_1$  is 1.10 and the dispersion is 45%. Since the median energy of the showers is  $10^{18.1}$ eV, the error in the  $S(600)$  determination by the  $20\text{km}^2$  array is rather large and hence the wide spread is reasonable.

In Figure 16, the spectrum obtained by the  $1\text{ km}^2$  array ( $E_1$ ) is shown with open squares and that by AGASA by closed squares. There is a difference in the overlapping energy region representing a 10% energy difference. In the same figure, results below  $10^{18}$ eV from several experiments are plotted. The Akeno energy spectrum is in good agreement with other experiments [31] from the *knee* to the second *knee* region, except Blanca [32] and DICE [33]. The comparison of the present results with other experiments in the highest energy region will be made elsewhere.

## 5 Conclusion

We have reevaluated the uncertainties in energy estimation using data accumulated over ten years. Table 2 summarizes the major systematics and uncertainties in energy estimation. Here, the symbol “+” means that currently assigned energies should be pushed up under a particular effect, and the symbol “−” represents a shift in the opposite direction. The probable overestimation of 10% due to shower front structure and delayed particles may be compensated for by the probable underestimation of the energy conversion factor by 10%, an effect resulting from the inclusion of the average altitude of AGASA and the proper definition of what is meant by a “single particle”. Adding uncertainties in quadrature, the systematic uncertainty in energy determination in the AGASA experiment is estimated to be  $\pm 18\%$  in total. Therefore, the currently assigned energies of the AGASA events have an accuracy of  $\pm 25\%$  in event-reconstruction resolution and  $\pm 18\%$  in systematics.

It should be noted that the Akeno-AGASA spectra cover over five decades in energy, connecting smoothly from the *knee* to a few times  $10^{20}$ eV, except for a 10% difference in energy in the  $10^{19}$ eV region. This may be due to the difference in the energy conversion relations for the experiments and is within the systematic errors evaluated here. It is concluded that there are surely events above  $10^{20}$ eV and the energy spectrum extends up to a few times  $10^{20}$ eV. The present highest energy event may only be limited by exposure. The next generation of experiments with much larger exposures are highly anticipated.

## Acknowledgements

We are grateful to Akeno-mura, Nirasaki-shi, Sudama-cho, Nagasaka-cho, Ohizumi-mura, Tokyo Electric Power Co. and Nihon Telegram and Telephone Co. for their kind cooperation. We are indebted to other members of the Akeno group in the maintenance of the AGASA array. We also thank Bruce Dawson for his kind advice in improvements of this article. This work is supported in part by JSPS (Japan Society for the Promotion of Science) grants in aid of Scientific Research #12304012.

## References

- [1] K. Greisen, *Rhys. Rev. Lett.* **16** (1966) 748.
- [2] G. T. Zatsepin and V. A. Kuz'min, *Zh. Eksp. Teor. Fiz.* **4** (1966) 114 [*JETP Letters* **4** (1966) 78].
- [3] M. Takeda et al., *Phys. Rev. Lett.* **81** (1998) 1163; N. Hayashida et al., *astro-ph/0008102*; The AGASA Collaboration, in *Proceedings of the 26th International Cosmic Ray Conference*, Utah, 1999, Vol. **3**, p. 252.
- [4] The High Resolution Fly's Eye Collaboration, A series of presentations in *Proceedings of the 27th International Cosmic Ray Conference*, Hamburg, 2001.
- [5] M. Ave et al., in *Proceedings of the 27th International Cosmic Ray Conference*, Hamburg, 2001, Vol. **1**, p. 381.
- [6] N. Hayashida et al., *Phys. Rev. Lett.* **73** (1994) 3491.
- [7] S. Yoshida et al., *J. Phys. G: Nucl. Part. Phys.* **20** (1994) 651.
- [8] S. Yoshida et al., *Astropart. Phys.* **3** (1995) 105.
- [9] M. Teshima et al., *Nucl. Instr. and Meth.* **A 247** (1986) 399.

- [10] N. Chiba et al., Nucl. Instr. and Meth. **A 311** (1992) 338.
- [11] H. Ohoka et al., Nucl. Instr. and Meth. **A 385** (1997) 268.
- [12] A. M. Hillas et al., in *Proceedings of the 12th International Cosmic Ray Conference*, Hobart, 1971, Vol. **3**, p. 1001.
- [13] T. Doi et al., in *Proceedings of the 24th International Cosmic Ray Conference*, Rome, 1995, Vol. **2**, p. 764.
- [14] N. Hayashida et al., in *Proceedings of the 26th International Cosmic Ray Conference*, Utah, 1999, Vol. **1**, p. 353.
- [15] H. Y. Dai et al., J. Phys. G: Nucl. Phys. **14** (1998) 793.
- [16] T. Hara et al., in *Proceedings of the 16th International Cosmic Ray Conference*, Kyoto, 1979, Vol. **8**, p. 175.
- [17] M. Nagano et al., J. Phys. Soc. Japan **53** (1984) 1667.
- [18] Akeno Internal Report, 1980, unpublished.
- [19] S. Shibata et al., in *Proceedings of the 9th International Cosmic Ray Conference*, London, 1965, Vol. **2**, p. 672.
- [20] M. Nagano et al., Astropart. Phys. **13** (2000) 277; FZKA 6191 (1998).
- [21] N. Sakaki et al., in *Proceedings of the 27th International Cosmic Ray Conference*, Hamburg, 2001, Vol. **1**, p. 329.
- [22] N. Sakaki et al., *in preparation*
- [23] K. Honda et al., in *Proceedings of the 20th International Cosmic Ray Conference*, Moscow, 1987, Vol. **6**, p. 83.; in *Proceedings of the 23rd International Cosmic Ray Conference*, Calgary, 1993, Vol. **4**, p. 311.
- [24] K. Honda et al., Phys. Rev. **D 56** (1997) 3833.
- [25] M. Teshima et al., J. Phys. G: Nucl. Phys. **12** (1986) 1097.
- [26] J. Linsley, in *Proceedings of the 18th International Cosmic Ray Conference*, La Jolla, 1985, Vol. **7**, p. 355.
- [27] K. Honda, *in preparation*.
- [28] T. Hara et al., in *Proceedings of the 18th International Cosmic Ray Conference*, Bangalore, 1983, Vol. **11**, p. 276.
- [29] M. Nagano et al., J. Phys. G: Nucl. Phys. **10** (1984) 1295.
- [30] M. Nagano et al., J. Phys. G: Nucl. Phys. **18** (1992) 423.



- [31] T. Abu-Zayyad et al., *Astrophys. J.* **557** (2001) 686.; H. Ulrich et al., in *Proceedings of the 27th International Cosmic Ray Conference*, Hamburg, 2001, Vol. **1**, p. 97.; A. Röhring et al., in *Proceedings of the 26th International Cosmic Ray Conference*, Salt Lake City, 1999, Vol. **1**, p. 214.; F. Aharonian et al., *Phys. Rev. D* **59** (1999) 092003.; Amenomori et al., *Astrophys. J.* **461** (1996) 408.; Asakimori et al., in *Proceedings of the 23rd International Cosmic Ray Conference*, Calgary, 1993, Vol. **2**, p. 25.; Ichimura et al., *Phys. Rev. D* **48** (1993) 1949.; Grigorov et al., in *Proceedings of the 12th International Cosmic Ray Conference*, Horbart, 1971, Vol. **5**, p. 1760.
- [32] J. W. Fowler et al., *Astropart. Phys.* **15** (2001) 49.; L. F. Fortson et al., in *Proceedings of the 12th International Cosmic Ray Conference*, Salt Lake City, 1999, Vol. **3**, p. 125.
- [33] D. B. Kieda and S. P. Swordy, in *Proceedings of the 12th International Cosmic Ray Conference*, Salt Lake City, 1999, Vol. **3**, p. 191.

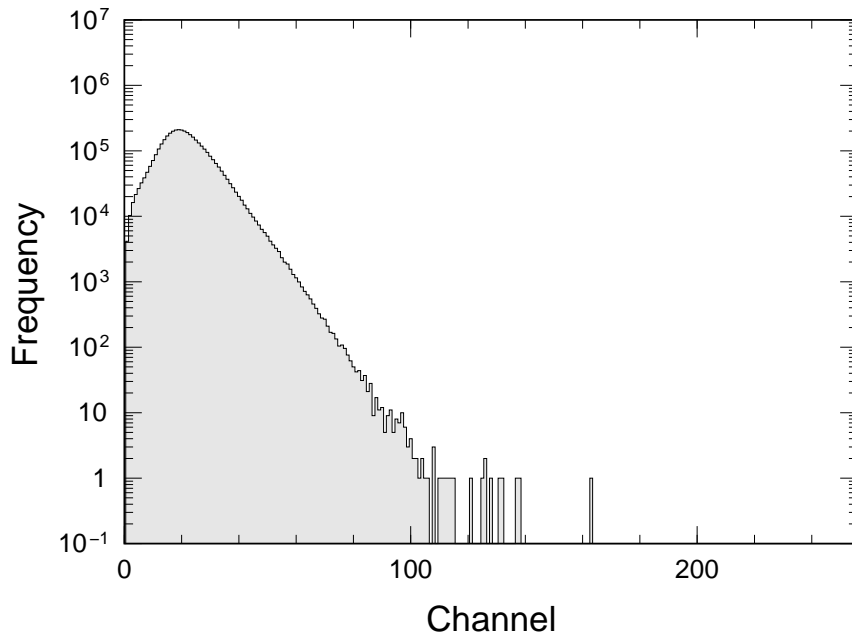


Fig. 1. An example of the pulse width distribution of a scintillation detector (TB22) for one run (about half a day). One channel corresponds to 500ns. This distribution is used to monitor the gain and the decay time of the exponential pulse.

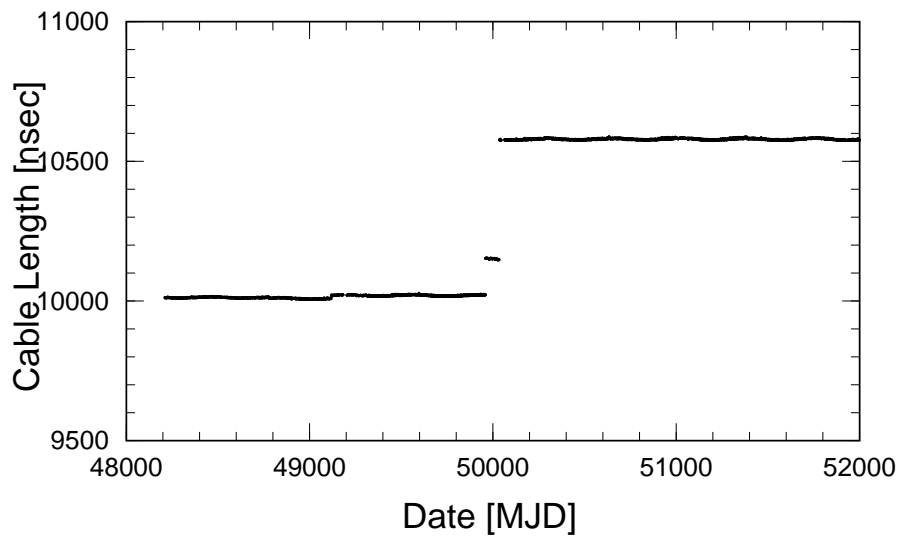


Fig. 2. An example of time variation of the cable delay (in nanoseconds) between a detector (TB22) and the control unit at a branch center. The discontinuity around 50,000 MJD is due to a change in the detector position and another one is due to a system upgrade in 1995.

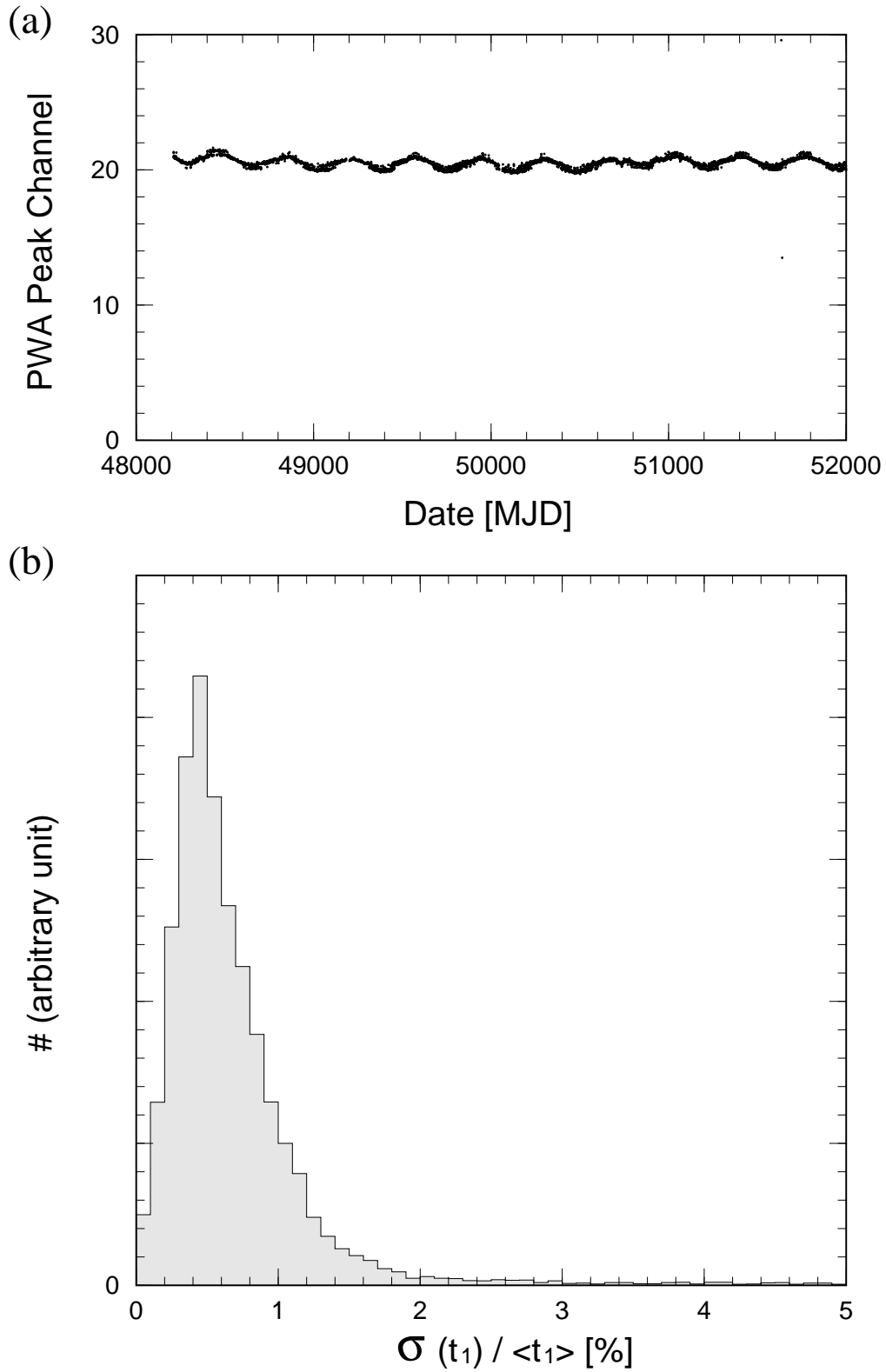


Fig. 3. (a) An example of the time variation in the PWA peak channel ( $t_1$ ) of a scintillation detector (TB22). (b) Distribution of  $\sigma(t_1)/\langle t_1 \rangle$  for all detectors, determined with the data from one month.

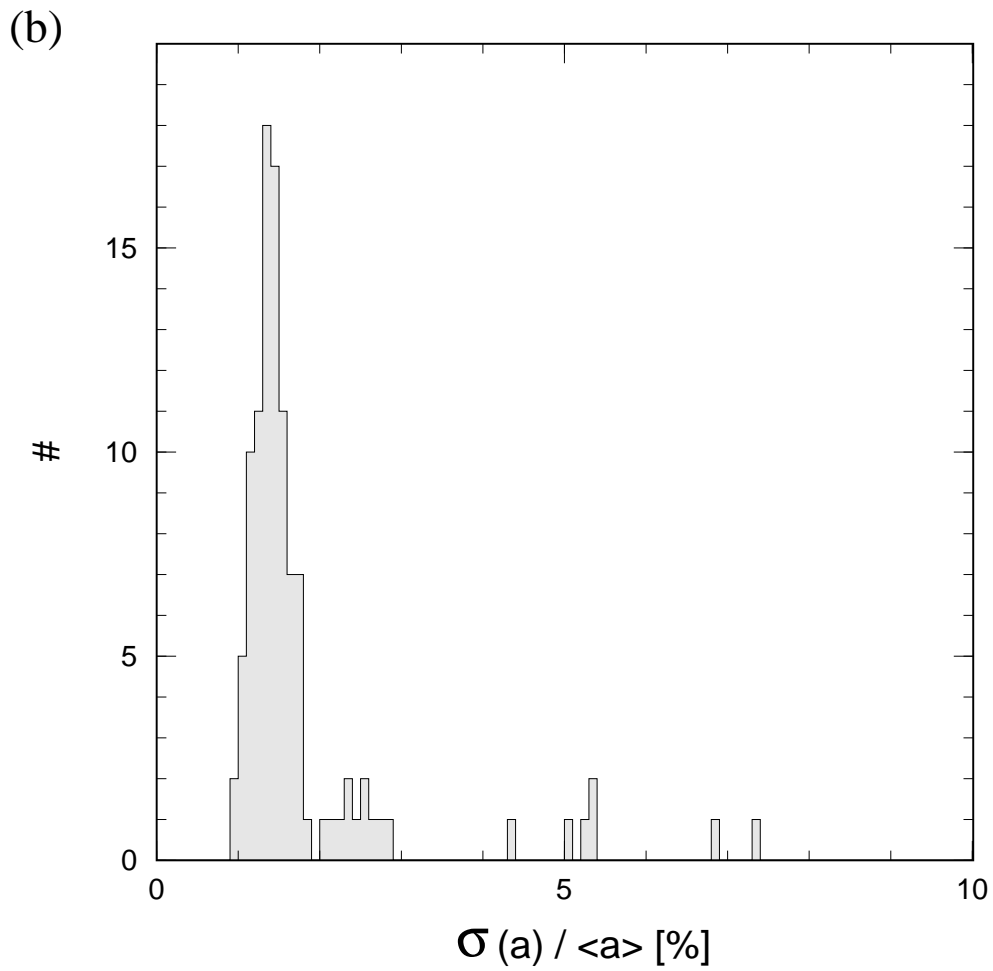
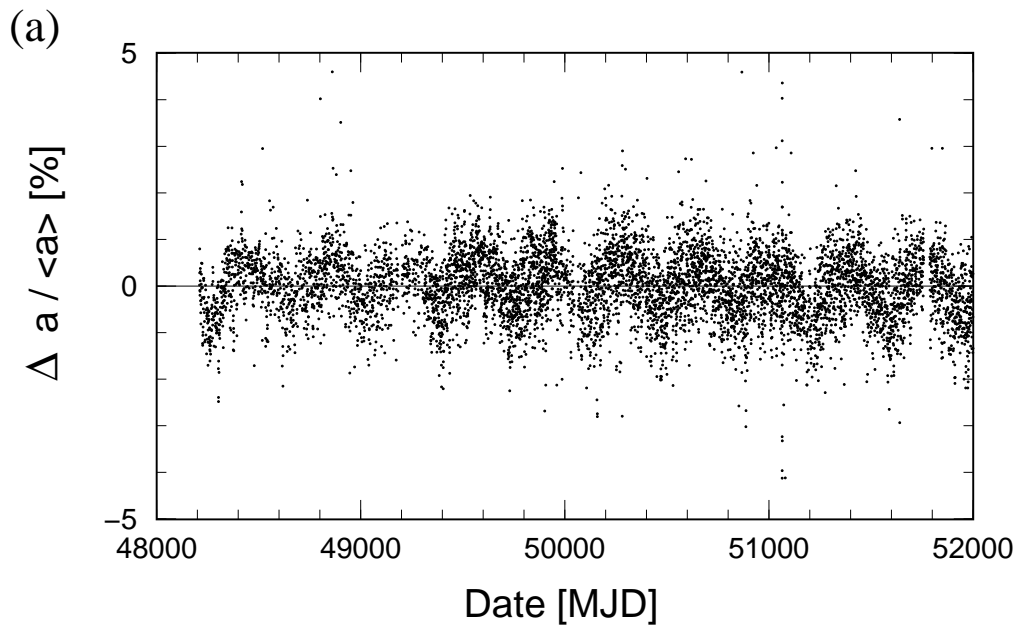


Fig. 4. (a) Time variation of  $\Delta a/a$  for a detector (TB22). (b) Distribution of  $\sigma(a)/\langle a \rangle$  for all detectors, determined with data from one month.

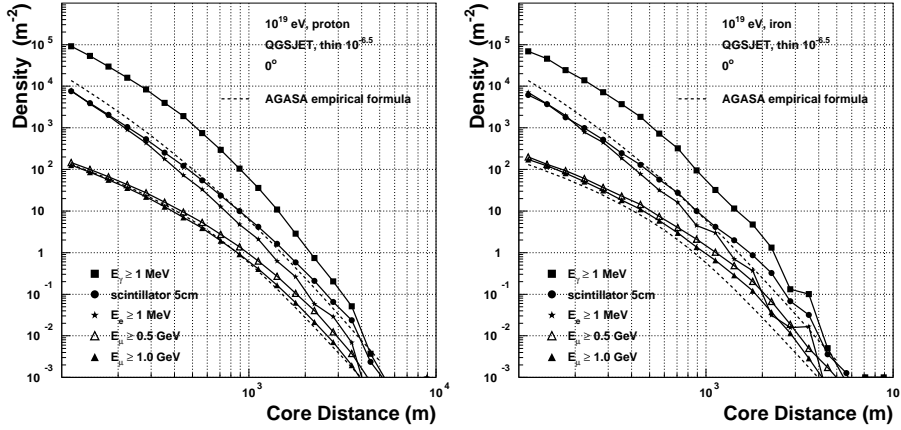


Fig. 5. The lateral distribution of energy deposited in an AGASA scintillator ( $\bullet$ ) in units of  $PH_{ave}^0$  is compared with the experimental lateral distribution of AGASA (dashed curve). The density of electrons ( $\geq 10\text{MeV}$ ), photons ( $\geq 1\text{MeV}$ ), muons ( $\geq 0.5\text{GeV}$ ) and muons ( $\geq 1\text{GeV}$ ) are also plotted. (Left: proton primary; Right: iron primary) [From Nagano et al., 1998]

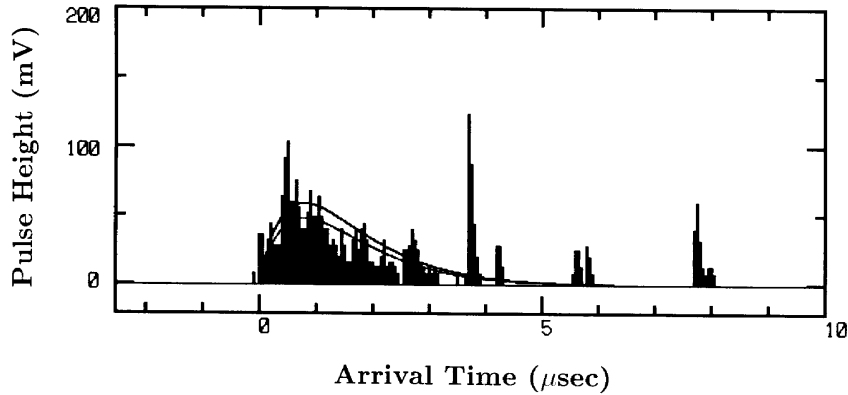


Fig. 6. Arrival time distribution of charged particles in a  $30\text{m}^2$  detector measured by a wave form recorder at  $1,920\text{m}$  from the core for a  $2 \times 10^{20}\text{eV}$  event. Solid curves correspond to  $t_0 = 800\text{ns}$ . The areas are normalized to the number of particles within  $2.5\mu\text{s}$  (87 particles) and  $3.5\mu\text{s}$  (115 particles), respectively. [From Hayashida et al., 1994]

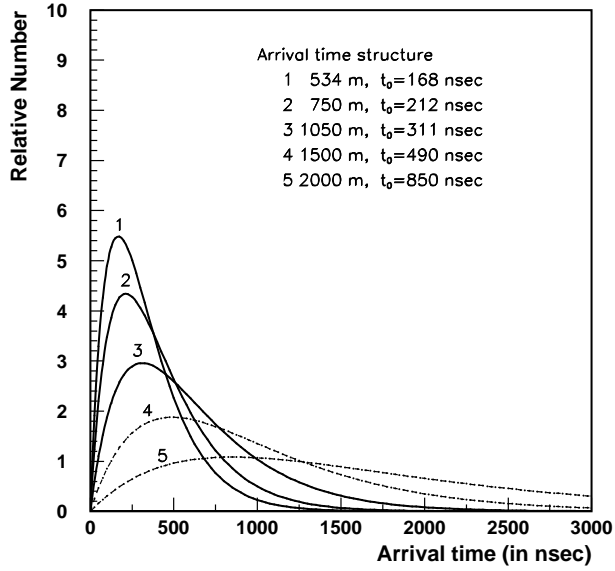


Fig. 7. Arrival time distribution of shower particles.  $t_0$  for 534m, 750m and 1,050m are determined experimentally with a 30m<sup>2</sup> scintillator [23], and those for 1,500m and 2,000m are extrapolated assuming  $\log t_0 \propto r$ .

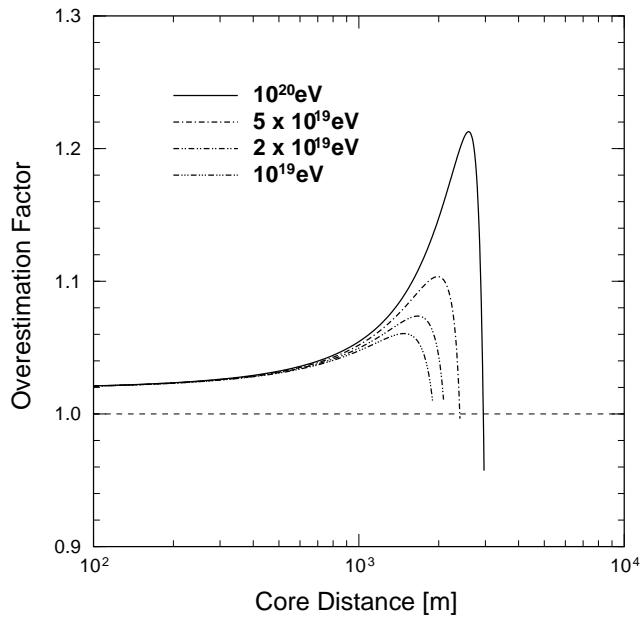


Fig. 8. Density overestimation due to the effect of shower front thickness estimated by considering the LDF profile for different energies. The drop at large core distance occurs at a radius where the expected particle count in a detector is one.

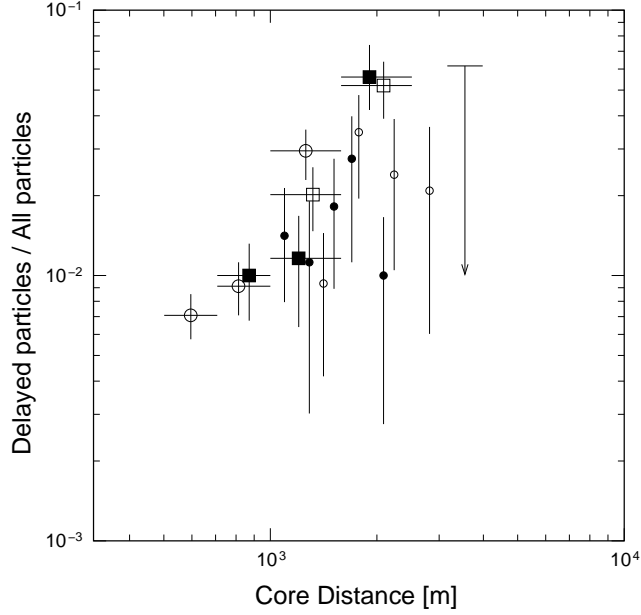


Fig. 9. Fraction of delayed particles to all shower particles. The current results are for  $t_D \geq 3\mu\text{s}$  and  $N_D \geq 1.0$  with three energy ranges of  $\log(\text{Energy [eV]}) = 18.5\text{--}19.0$  (big open circles),  $19.0\text{--}19.4$  (big open squares) and above  $19.4$  (big closed squares). The previous Akeno result by Teshima et al. [25] (small open circles), and the result by Linsley [26] (small closed circles) are for  $t_D \geq 4\mu\text{s}$  and  $N_D \geq 3.0$  with energies around  $10^{18}\text{eV}$ .

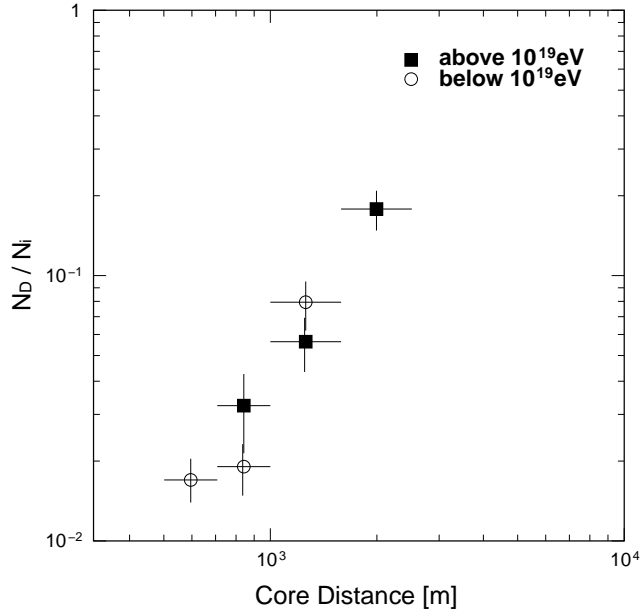


Fig. 10. Core distance dependence of the ratio  $N_D/N_i$ .

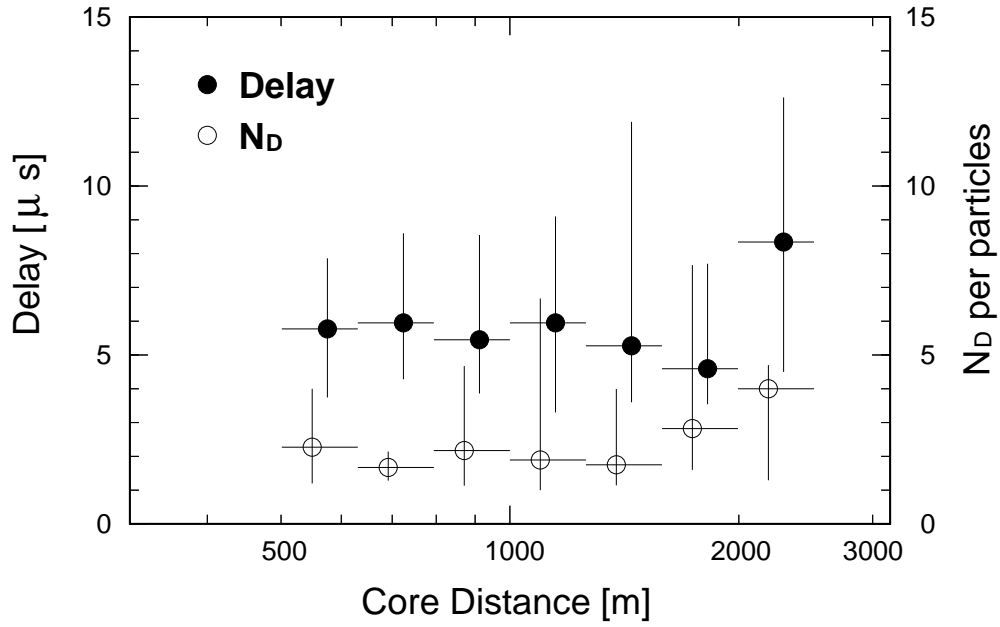


Fig. 11. Delay time and  $N_D$  of delayed particles as a function of core distance. Vertical bars indicate the 68% confidence limits in each bin. Data points within each bin range from 15 to 30, except for largest core distance bin (3 data points).

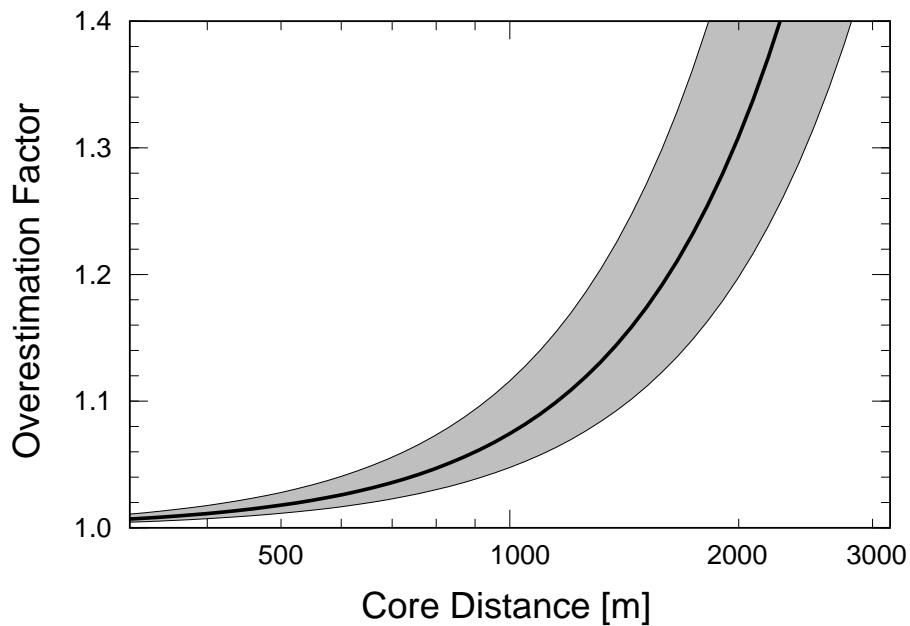


Fig. 12. Overestimation factor due to delayed particles as a function of core distance. The solid line indicates the  $OF$  values at each core distance with  $t_D = 6\mu$ s and their uncertainties are shown by the shaded region.



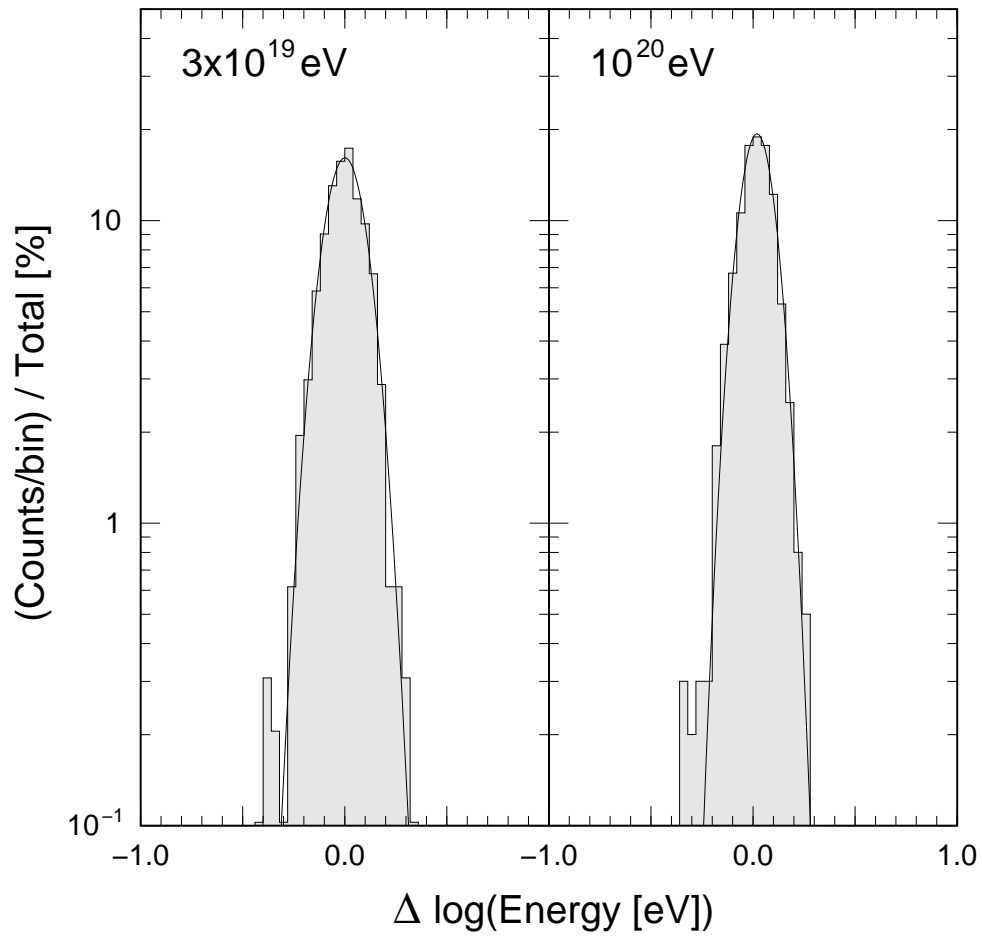


Fig. 13. Accuracy of energy determination for  $3 \times 10^{19} \text{ eV}$  and  $10^{20} \text{ eV}$  showers with zenith angles less than  $45^\circ$ . The solid curve indicates the Gaussian distribution fitted to the histogram.

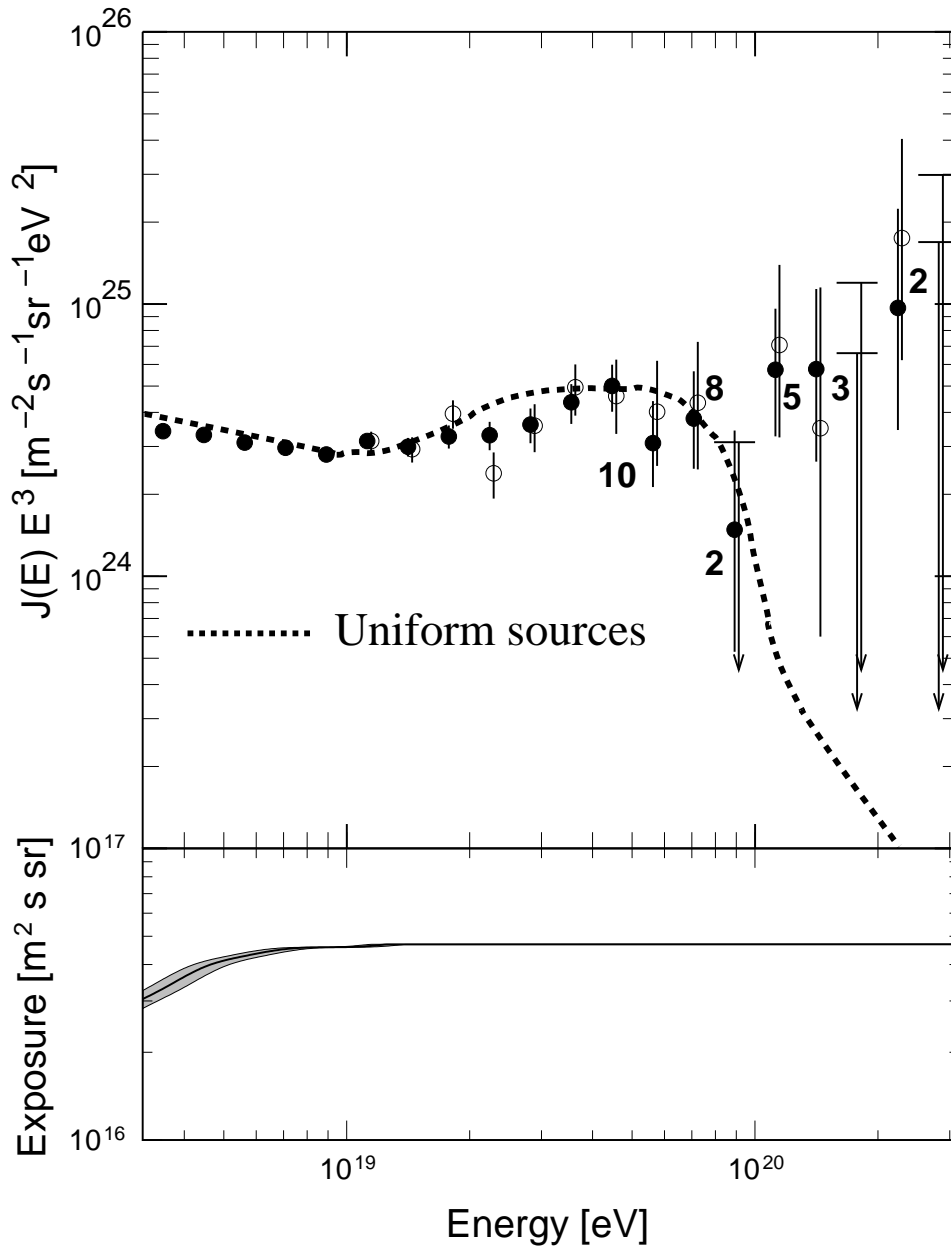


Fig. 14. Energy spectrum determined by AGASA and the exposure with zenith angles smaller than  $45^\circ$  up until July 2001. (Open circles: well contained events; Closed circles: all events) The vertical axis is multiplied by  $E^3$ . Error bars represent the Poisson upper and lower limits at 68% confidence limit and arrows are 90% C.L. upper limits. Numbers attached to the points show the number of events in each energy bin. The dashed curve represents the spectrum expected for extragalactic sources distributed uniformly in the Universe, taking account of the energy determination error. The uncertainty in the exposure is shown by the shaded region.

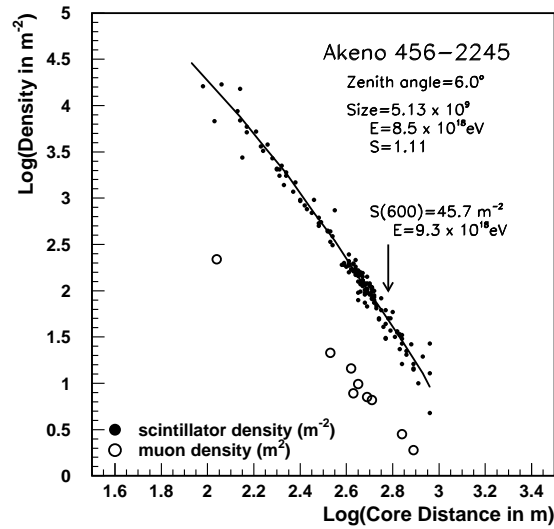


Fig. 15. Comparison of energies determined from  $N_e$  and  $S(600)$  for one of the largest events landing inside the  $1 \text{ km}^2$  array.

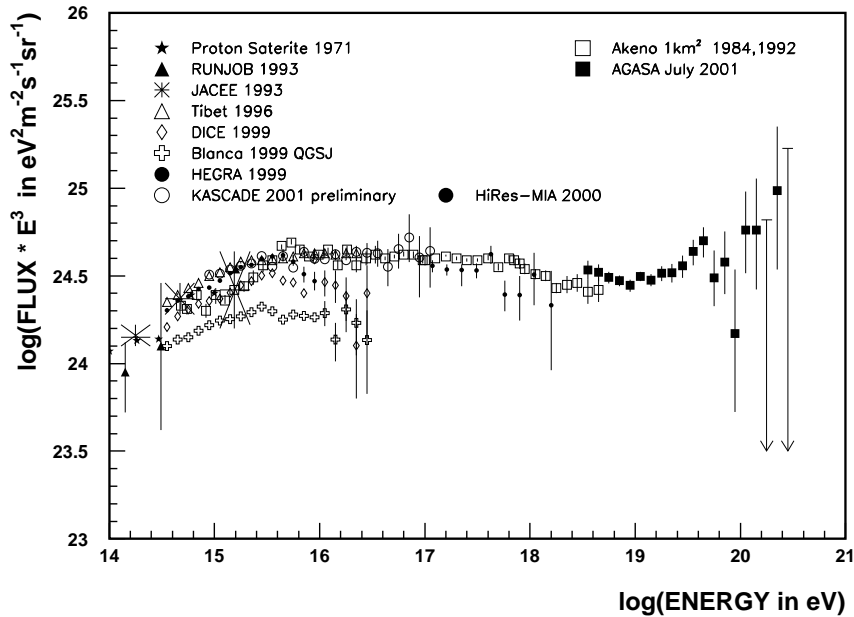


Fig. 16. Cosmic ray energy spectrum over a wide energy range. The present AGASA energy spectrum is shown by closed squares. The spectrum from the Akeno  $1 \text{ km}^2$  array is shown by open squares. The Akeno-AGASA energy spectrum covers more than 5 decades of energy and is in reasonable agreement with most energy spectra below  $10^{18} \text{ eV}$ .

Table 1

Energy conversion from  $S(600)$ . The column “Single Particle” describes the definition of “a single particle” used in the evaluation of  $S(600)$ . Each formula is evaluated at the altitude given in the column “Altitude”.

Simulation Code	Single Particle	Altitude	Interaction Model	Primary Composition	$E = a \times 10^{17} \cdot S_0(600)^b$		Citation
					$a$	$b$	
COSMOS	“electrons”	900m	QCDJET	p	2.03	1.02	[15]
CORSIKA	$PH_{peak}^0$	900m	QGSJET	p	2.07	1.03	[20]
				Fe	2.24	1.00	
			SIBYLL	p	2.30	1.03	
				Fe	2.19	1.01	
AIRES	$PW_{peak}^\theta$	667m	QGSJET	p	2.17	1.03	[21]
				Fe	2.15	1.01	
			SIBYLL	p	2.34	1.04	
				Fe	2.24	1.02	

Table 2

Major systematics of AGASA.

Detector:	
detector absolute gain	$\pm 0.7\%$
detector linearity	$\pm 7\%$
detector response (box, housing, ...)	$\pm 5\%$
Air shower phenomenology:	
lateral distribution function	$\pm 7\%$
$S(600)$ attenuation	$\pm 5\%$
shower front structure	$- 5\% \pm 5\%$
delayed particles	$- 5\% \pm 5\%$
Energy estimator $S(600)$ :	
interaction models, chemical compositions (p/Fe),	} $+10\% \pm 12\%$
simulation codes, height correction,	
$S(600)$ fluctuation	
Total	$\pm 18\%$